








Article

Hydrogel Membranes from Chitosan-Fish Gelatin-Glycerol for Biomedical Applications: Chondroitin Sulfate Incorporation Effect in Membrane Properties

Andreas Karydis-Messinis ^{1,*}, Dimitrios Moschovas ¹, Maria Markou ², Kyriaki Tsirka ¹ , Christina Gioti ¹, Eleni Bagli ², Carol Murphy ², Aris E. Giannakas ³ , Alkis Paipetis ¹ , Michael A. Karakassides ¹ , Apostolos Avgeropoulos ¹ , Constantinos E. Salmas ^{1,*}  and Nikolaos E. Zafeiropoulos ^{1,*} 

¹ Department of Material Science and Engineering, University of Ioannina, 45110 Ioannina, Greece; dmoschov@uoi.gr (D.M.); ktsirka@uoi.gr (K.T.); christina.a.gioti@gmail.com (C.G.); paipetis@uoi.gr (A.P.); mkarakas@uoi.gr (M.A.K.); aavger@uoi.gr (A.A.)

² Biomedical Research Institute (BRI)-FORTH, 45110 Ioannina, Greece; mmarkou92@gmail.com (M.M.); elenibgl@hotmail.com (E.B.); carol_murphy@bri.forth.gr (C.M.)

³ Department of Food Science and Technology, University of Patras, 30100 Agrinio, Greece; agiannakas@upatras.gr

* Correspondence: karydis.and@gmail.com (A.K.-M.); ksalmas@uoi.gr (C.E.S.); nzafiro@uoi.gr (N.E.Z.)

Abstract: Chondroitin sulfate (ChS), chitosan (Chi), and fish gelatin (FG), which are byproducts of a fish-treatment small enterprise, were incorporated with glycerol (Gly) to obtain dense hydrogel membranes with reduced brittleness, candidates for dressing in wound healing applications. The mechanical properties of all samples were studied via Dynamic Mechanical Analysis (DMA) and tensile tests while their internal structure was characterized using Attenuated Total Reflectance-Fourier Transform Infrared Spectroscopy (ATR-FTIR) and X-ray Diffraction (XRD) instruments. Their surface morphology was analyzed by ThermoGravimetric Analysis (TGA) method, while their water permeability was estimated via Water Vapor Transmission Rate (WVTR) measurements. Wettability and degradation rate measurements were also carried out. Characterization results indicated that secondary interactions between the natural polymers and the plasticizer create the hydrogel membranes. The samples were amorphous due to the high concentration of plasticizer and the amorphous nature of the natural polymers. The integration of ChS led to decreased decomposition temperature in comparison with the glycerol-free sample, and all the materials had dense structures. Finally, the in vitro endothelial cell attachment studies indicate that the hydrogel membranes successfully support the attachment and survival of primary on the hydrogel membranes and could be appropriate for external application in wound healing applications as dressings.

Keywords: chitosan; fish gelatin; chondroitin sulfate; hydrogel membranes; wound dressing; in vitro cell colonization; gelatin glycerol; biomedical applications; membranes; biomaterials



Citation: Karydis-Messinis, A.; Moschovas, D.; Markou, M.; Tsirka, K.; Gioti, C.; Bagli, E.; Murphy, C.; Giannakas, A.E.; Paipetis, A.; Karakassides, M.A.; et al. Hydrogel Membranes from Chitosan-Fish Gelatin-Glycerol for Biomedical Applications: Chondroitin Sulfate Incorporation Effect in Membrane Properties. *Gels* **2023**, *9*, 844. <https://doi.org/10.3390/gels9110844>

Academic Editor: Kummara Madhusudana Rao

Received: 20 September 2023

Revised: 18 October 2023

Accepted: 23 October 2023

Published: 25 October 2023



Copyright: © 2023 by the authors. Licensee MDPI, Basel, Switzerland. This article is an open access article distributed under the terms and conditions of the Creative Commons Attribution (CC BY) license (<https://creativecommons.org/licenses/by/4.0/>).

1. Introduction

In recent years, wound management methods have evolved considerably due to the deeper understanding of the molecular and cellular processes that take place during the healing process and the factors controlling it. Consequently, the design and functionality of the wound healing patches has turned to the creation of multi-functional materials. Wounds are dissimilar in nature and characteristics and depend on a variety of factors, such as origin (burn, surgery, incision, etc.), the state of health of the person and, the manifestation of infection [1]. Therefore, the requirements of the wound for a wound dressing, depend entirely on its type. Modern patches must be biocompatible, non-cytotoxic, non-inflammatory, have a rate of degradation commensurate with the rate of new tissue formation and prevent/treat possible infections [2,3]. The most important property required for wound dressings and especially those intended for burns, is the ability to absorb

and retain water. For this type of damage, it is necessary to keep the wound hydrated, to absorb its secretions and accelerate the healing process by avoiding cellular dehydration in order to promote collagen synthesis and angiogenesis [4]. Proper hydration increases the healing rate, protects the wound from infections, and reduces pain [5]. The synthetic process of the patches must be simple, fast, and economically advantageous. They must also provide mechanical stability to the wound and be easily sterilized [1].

Hydrogels are hydrophilic macromolecular networks, synthesized through the formation of physical and chemical crosslinking [6]. The characteristics of the hydrogels depend significantly on the polymers used (natural, synthetic or a combination of the two) and the interactions between them [7]. The formation of covalent bonds improves the mechanical properties; however, it leads to a reduction in the degradation rate, affecting the biocompatibility of the materials synthesized [8,9]. Physical crosslinking leads to the formation of a relatively weak network through molecular and/or secondary interactions such as electrostatic interactions, hydrogen bonds and hydrophobic interactions [7,10]. The disruption of the network in the case of physically crosslinked hydrogels can result from changes in various conditions (pH, temperature, solvent) giving these materials excellent properties (controlled release of bioactive agents and drugs). The main advantage of hydrogels synthesized through physical crosslinking, is biocompatibility because no crosslinker is required for the network formation and the potential toxicity problems that can be caused by cross-linkers (genipin, glutaraldehyde, etc.) used during chemical crosslinking are avoided [7,8]. Polysaccharide and protein-based materials have functional groups, such as hydroxyl groups, carboxyl groups and amino groups, providing binding sites appropriate to form secondary interactions. The weak interactions developed through physical crosslinking stabilize the network and the dissolution of the hydrogel is avoided.

Natural polymers like chitosan, gelatin and collagen are widely used in wound management due to their attractive properties (biodegradation, biocompatibility etc.) [11,12]. However, their use is limited to developing porous materials through complicated synthetic routes. The use of dense, non-porous hydrogel membranes in applications such as wound healing is also limited. Sharma et al. developed a polyelectrolyte complex (PEC) using chitosan and chondroitin sulfate for effective management of chronic wounds [13] Liu et al. developed biodegradable and cytocompatible coatings or the Prevention of Implant-Associated Infection [14]. Lu et al. developed chitosan hydrogels crosslinked with the synthetic polymer PEG as candidate antibacterial wound dressings [15].

In the present study hydrogel membranes were synthesized via a green process and characterized via various instrumental and in-vitro methods. These hydrogel membranes consisting of bio-based and bio-degradable materials such as Chitosan (Chi), Fish Gelatin (FG), Chondroitin Sulfate (ChS), and Glycerol (Gly). The novelty of this work is the development of dense hydrogel membranes by the incorporation of the ChS biomaterial in a ChS-free material developed in a previous published work [16], to further improve some properties. The comparison of these two groups of materials shown improvement of cell-adhesion and water-uptake properties, which are significant properties for wound healing applications, while the mechanical properties remain stable. The objective of the current work is to study the effect of ChS integration on the overall properties of the materials. ChS was selected because of its antioxidant, anti-inflammatory and anti-apoptotic properties [17,18]. ChS has a wide range of bioactivities including tissue regeneration, intracellular signaling, cell proliferation, and cell adhesion [19,20]. Fialkova et al. [21], reported that topical application of ChS on the wound surface of rats after surgery resulted in a significant reduction in edema of the tissue surrounding the wound compared to the wound where ChS was not used. It was also shown that the application of ChS led to a reduction in hyperemia and wound secretions in relation to wounds where ChS not applied. However, the use of ChS in wound healing applications is still limited.

2. Results and Discussion

2.1. ATR-FTIR Spectroscopy

Components' inter- and intra-molecular secondary interactions were studied using an ATR-FTIR instrument. ChS, Chi₃₀Gly₇₀, Chi₁₃FG₅₃Gly₃₄ (chitosan/fish-gelatin/glycerol), and Chi₁₃FG₅₀ChS₃Gly₃₄ spectra, obtained from this instrument, are shown in Figure 1. Figure 1a presents the spectrum of the ChS membrane. The broad peak between 3600–3200 cm⁻¹ arises from the stretching vibrations of the OH and NH groups [22]. The peak observed at 1610 cm⁻¹ is representative of carbonyl groups (C=O). The peak at 1228 cm⁻¹ is ascribed to then negatively charged group -OSO³⁻ of ChS [20]. The peaks at 1631 cm⁻¹, 1637 cm⁻¹ and 1637 cm⁻¹ appear in Figures 1b, 1c and 1d respectively, attributed to stretching vibrations of C=O. The peaks revealed at 1553 cm⁻¹, 1543 cm⁻¹ and 1543 cm⁻¹, ascribed to bending vibrations of N-H, while the peaks at 1240 cm⁻¹, 1238 cm⁻¹ and 1244 cm⁻¹ indicate bending vibrations of N-H groups [23]. The observed shifts of the peaks in the spectra Figure 1c relative to the spectra Figure 1b, indicate hydrogen bonds formation between chitosan and fish gelatin [23–25]. The shifts of Figure 1d relative to the spectra Figure 1b, designate CONH₂ formation (interactions between chitosan and chondroitin sulfate). The increased intensity of the peak at 1244 cm⁻¹ in Figure 1d confirm the interactions between chondroitin sulfate and chitosan [20,23]. The observed peaks at 2926 cm⁻¹ (Figure 1b), at 2936 cm⁻¹ (Figure 1c) and 2934 cm⁻¹ (Figure 1d) are representative of asymmetrical stretching vibrations of C-H groups while the peaks at 2879 cm⁻¹ (Figure 1b), at 2876 cm⁻¹ (Figure 1c) and 2883 cm⁻¹ (Figure 1d) arises from symmetrical stretching vibrations of C-H groups of chitosan. The broad peaks between 3500–3000 cm⁻¹ indicate the existence of stretching vibrations of O-H and N-H groups [23]. The shifts designate ionic interactions between the natural polymers and hydrogel membrane formation from polyelectrolytes.

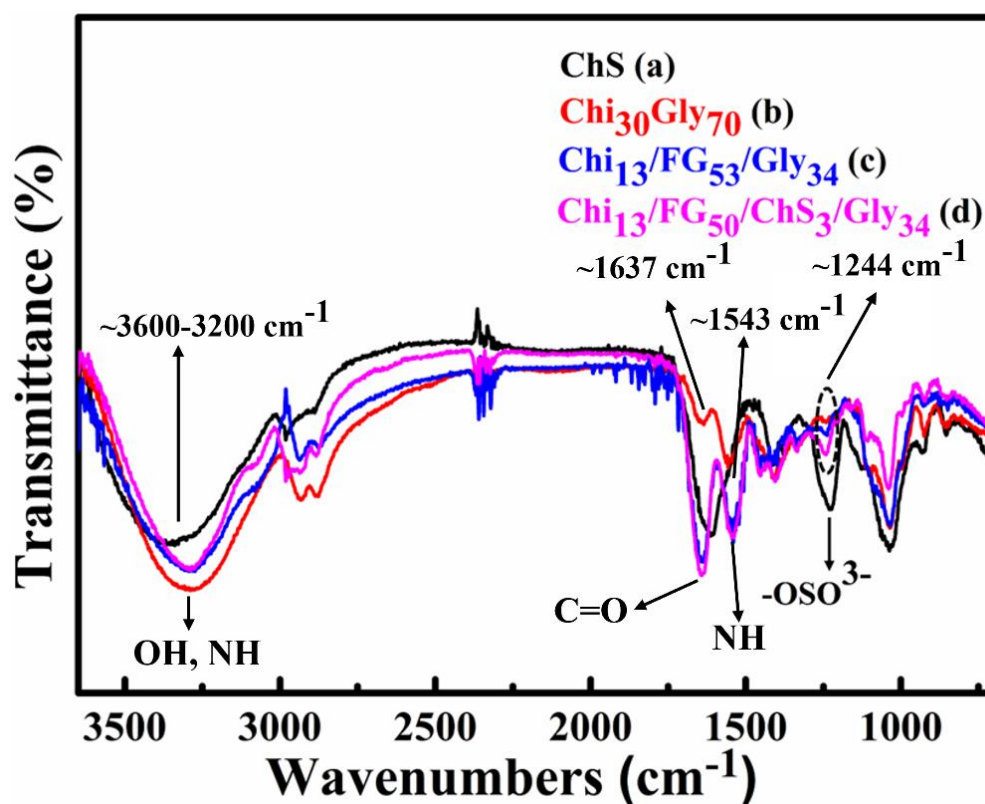


Figure 1. FTIR spectra of chondroitin sulfate (ChS) (a), chitosan/glycerol (Chi₃₀Gly₇₀) (b), chitosan/fish gelatin/glycerol membrane (Chi₁₃FG₅₃Gly₃₄) (c) and chitosan/fish gelatin/chondroitin sulfate/glycerol membrane (Chi₁₃FG₅₀ChS₃Gly₃₄) (d).

2.2. XRD Analysis

The XRD patterns of ChS, Chi₁₃FG₅₃Gly₃₄ and Chi₁₃FG₅₀ChS₃Gly₃₄ are shown in Figure 2. Figure 2a represents the XRD pattern of ChS. The broad peak appears at $2\theta = 24^\circ$, confirms the amorphous nature of polysaccharide. The amorphous nature of chondroitin sulfate ascribed to the low crystallinity profile of the main chain of the natural polymer [26–28]. The rest of the materials showed a similar behavior (Figure 2b,c). The amorphous nature of the natural polymers utilized in the present work as well as the high concentration of the plasticizer, led to the development of amorphous materials [29].

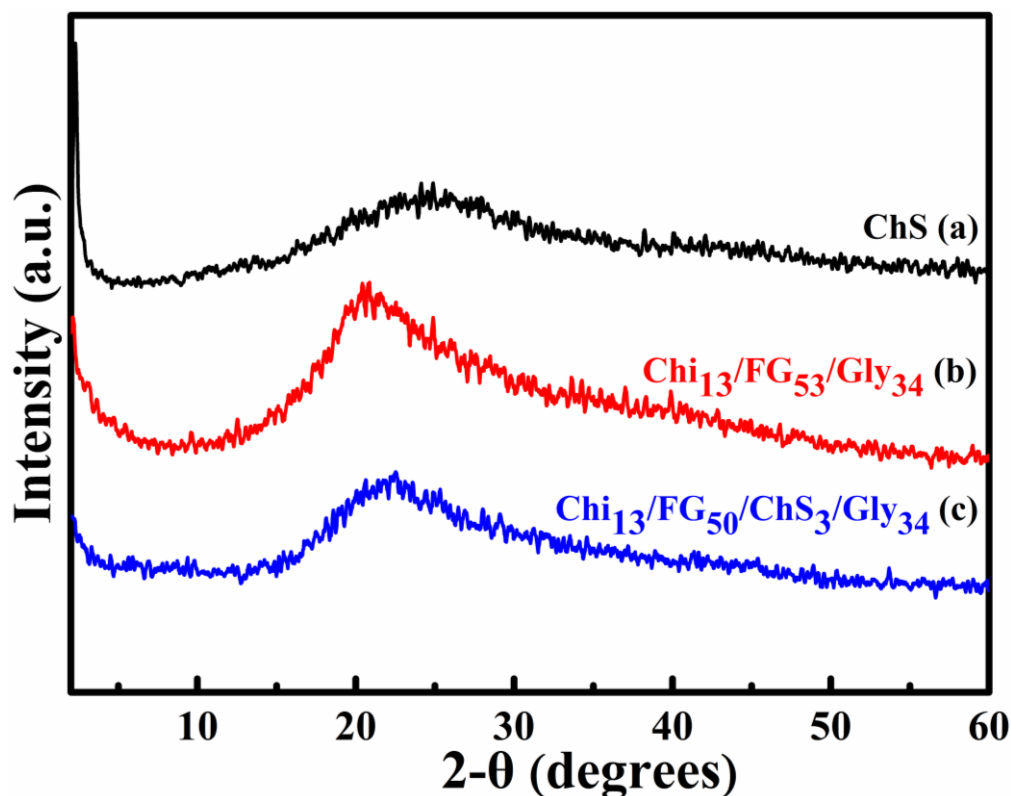


Figure 2. XRD diffractograms of ChS (a), Chi₁₃FG₅₃Gly₃₄ (b) and Chi₁₃FG₅₀ChS₃Gly₃₄ (c).

2.3. TGA Measurements

The results of the TGA measurements of Chi₁₃FG₅₃Gly₃₄ and Chi₁₃FG₅₀ChS₃Gly₃₄ (before and after the integration of ChS) are depicted in Figure 3. In all the thermograms a mass loss in the range between ~ 80 – 150°C is observed, showing the materials' water removal. A notable mass loss occurs in the temperature range 220 – 400°C . This loss is ascribed to materials' functional groups disintegration and because of this the materials' disruption. Figure 3a shows the thermal decomposition of ChS-free material while Figure 3b the results of ChS-containing material, respectively. In the first case the decomposition begins at 200°C while after the integration of chondroitin sulfate, begins at 180°C . The addition of chondroitin sulfate led to decreased thermal stability perhaps due to poor miscibility of the components. The remaining 20–30% of the mass is ascribed to remaining ash.

2.4. DMA Measurements

Dynamic mechanical analysis was used to examine the thermomechanical response and the miscibility of the blends. In Figure 4 the results of the storage modulus as a function of temperature of the hydrogel membranes Chi₂₀FG₂₀ChS₅Gly₅₅ (Figure 4a), Chi₁₇FG₃₄ChS₄Gly₄₅ (Figure 4b), Chi₁₃FG₅₀ChS₃Gly₃₄ (Figure 4c) and Chi₁₃FG₅₃Gly₃₄ (Figure 4d) are shown. All the materials showed a similar behavior in the range between -70 – 120°C . The integration of chondroitin sulfate did not improve the mechanical proper-

ties of the materials, probably due to the low concentration used. The observed increase in storage modulus after $\sim 80^\circ\text{C}$, is attributed to the removal of water which acts as a plasticizer in these materials [30].

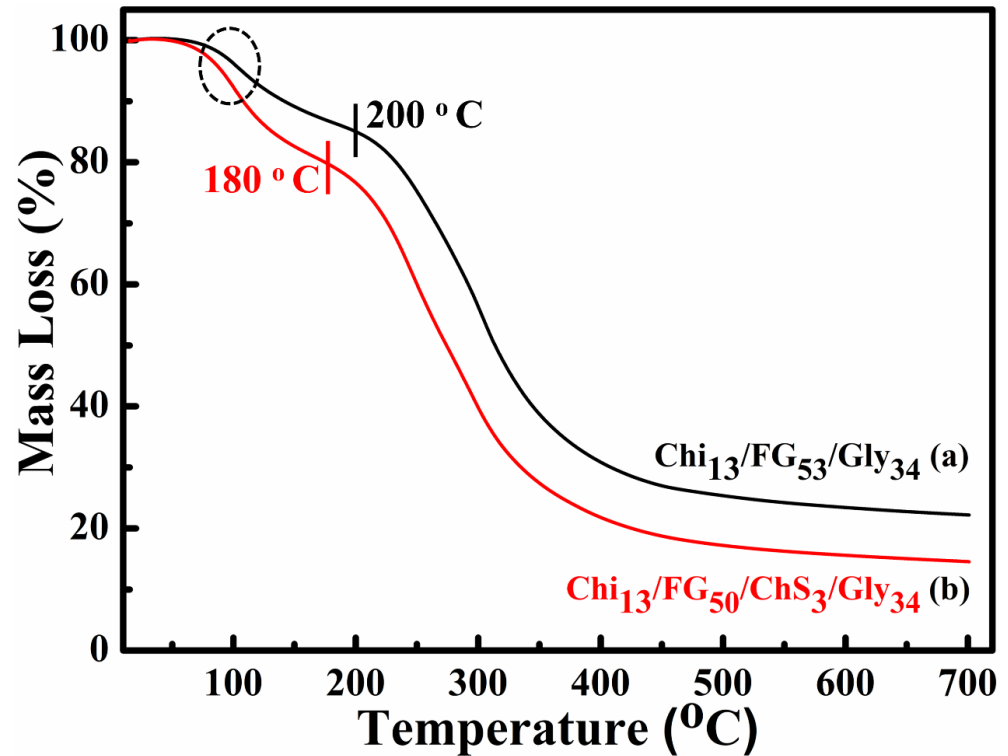


Figure 3. TGA thermograms of $\text{Chi}_{13}\text{FG}_{53}\text{Gly}_{34}$ (a) and $\text{Chi}_{13}\text{FG}_{50}\text{ChS}_3\text{Gly}_{34}$ (b).

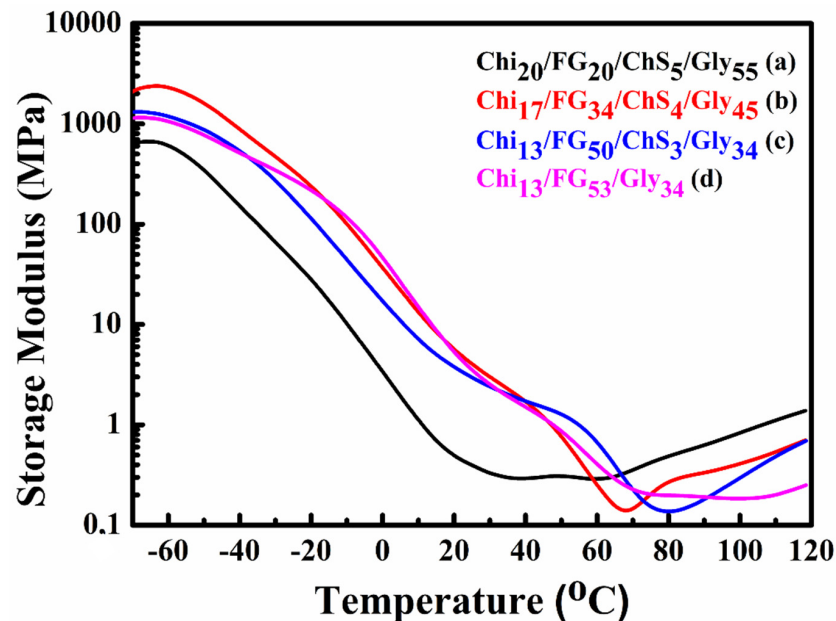


Figure 4. $\text{Chi}_{20}\text{FG}_{20}\text{ChS}_5\text{Gly}_{55}$ storage modulus and DMA results presented on graphs (a), $\text{Chi}_{17}\text{FG}_{34}\text{ChS}_4\text{Gly}_{45}$ (b), $\text{Chi}_{13}\text{FG}_{50}\text{ChS}_3\text{Gly}_{34}$ (c) and $\text{Chi}_{13}\text{FG}_{53}\text{Gly}_{34}$ (d) hydrogel membrane.

Figure 5 shows the tan delta variation depending on temperature increase. The glass transition temperatures (T_g s) of the hydrogel membranes $\text{Chi}_{20}\text{FG}_{20}\text{ChS}_5\text{Gly}_{55}$ (Figure 5a), $\text{Chi}_{17}\text{FG}_{34}\text{ChS}_4\text{Gly}_{45}$ (Figure 5b), $\text{Chi}_{13}\text{FG}_{50}\text{ChS}_3\text{Gly}_{34}$ (Figure 5c) and $\text{Chi}_{13}\text{FG}_{53}\text{Gly}_{34}$ (Figure 5d) are located at 0.9°C , 4.4°C and -8.7°C respectively. The peaks appear in

the range between 40–80 °C at Figure 5b–d, are attributed to the poor miscibility of the natural polymers with the plasticizer and are the T_g s of chitosan and fish gelatin which did not interact with chondroitin sulfate and glycerol. In Figure 5a only one T_g is observed, indicating the development of a single-phase system.

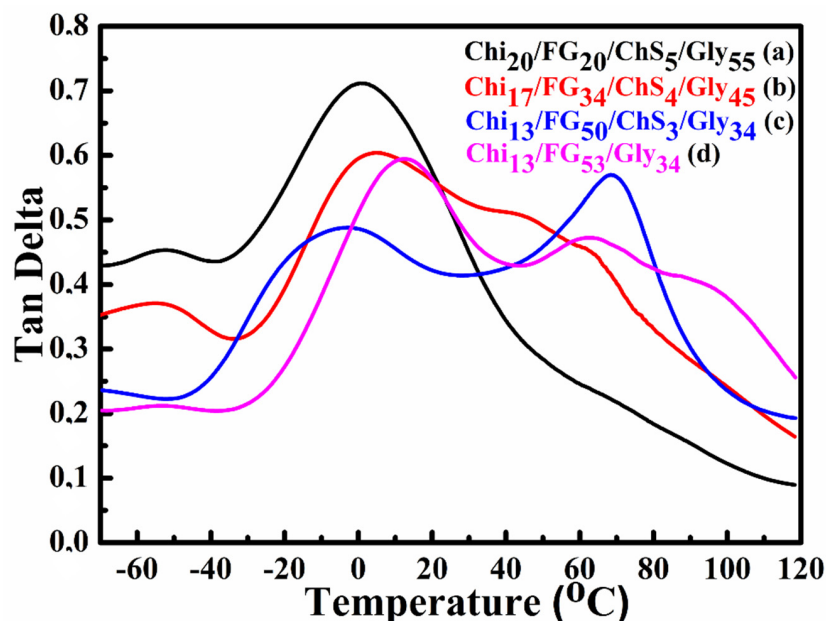


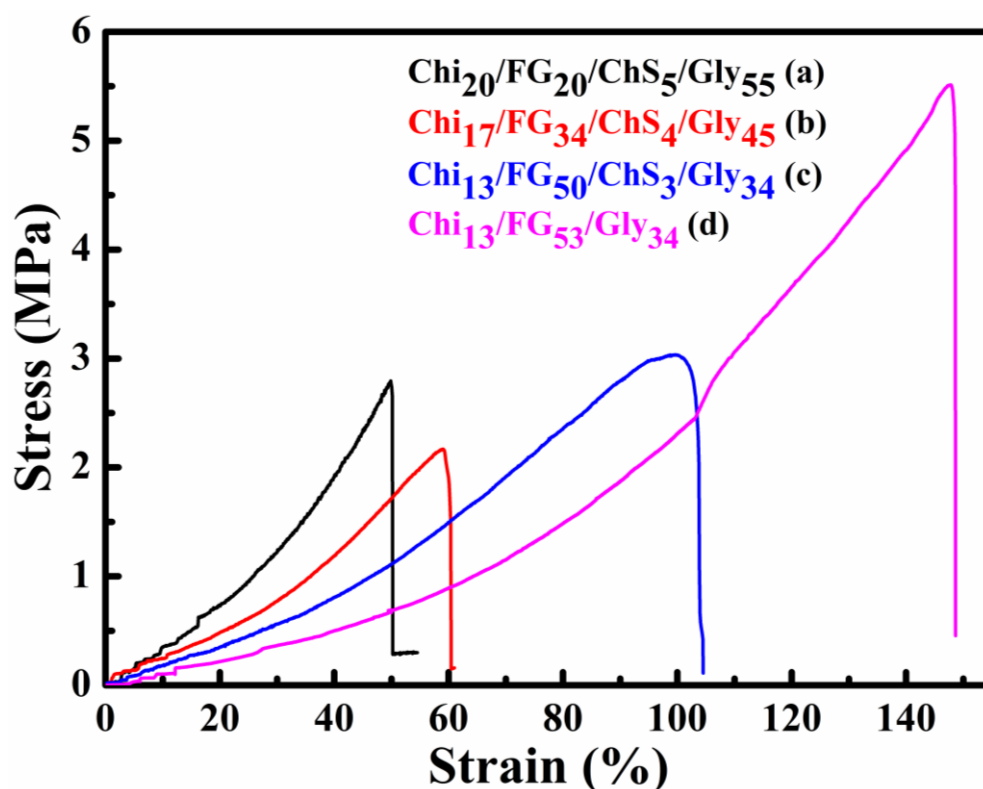
Figure 5. Tan delta plots of Chi₂₀FG₂₀ChS₅Gly₅₅ (a), Chi₁₇FG₃₄ChS₄Gly₄₅ (b), Chi₁₃FG₅₀ChS₃Gly₃₄ (c) and Chi₁₃FG₅₃Gly₃₄ (d) hydrogel membrane.

2.5. Tensile Properties

The average tensile strength and the respective strain to failure of the hydrogel membranes are summarized in Table 1 and indicative stress-strain plots from the tested membranes are presented in Figure 6. The Chi₁₃FG₅₃Gly₃₄ can be regarded as the reference membrane with an average stress of 6.03 MPa and a strain to failure equal to 152.95%. According to the tensile tests the incorporation of ChS in the blend caused a decrease of both the strength and the strain to failure values of the membranes. The smallest deterioration in terms of strength was observed for the Chi₁₇FG₃₄ChS₄Gly₄₅ specimens in comparison to the reference membrane. On the other hand, the smallest decrease in the strain to failure values was observed for the Chi₁₃FG₅₀ChS₃Gly₃₄ in comparison to the reference membranes. An interesting observation is that although all the other membranes failed in an abrupt manner, as indicated by curves Figure 6a,b,d, whereby a maximum stress was observed and the specimens then ruptured suddenly, the Chi₁₃FG₅₀ChS₃Gly₃₄ specimens failed more gradually, sustaining the maximum stresses for an amount of strain. This different and more ductile failure type was consistently observed in all the tested specimens of this category. Literature values report normal human skin tensile strength in the range 2.5–16 MPa and strain at break percentage 70% [31]. Such results are in agreement with the experimental data of this study.

Table 1. Mechanical properties of the hydrogel membranes Chi₂₀FG₂₀ChS₅Gly₅₅, Chi₁₇FG₃₄ChS₄Gly₄₅, Chi₁₃FG₅₀ChS₃Gly₃₄ and Chi₁₃FG₅₃Gly₃₄.

Specimen	Stress (MPa)	Strain (%)	% Change in Stress	% Change in Strain
Chi ₂₀ FG ₂₀ ChS ₅ Gly ₅₅	2.64 ± 0.23	52.87 ± 2.61	−56.22	−65.43
Chi ₁₇ FG ₃₄ ChS ₄ Gly ₄₅	3.33 ± 1.00	62.35 ± 1.46	−44.78	−59.24
Chi ₁₃ FG ₅₀ ChS ₃ Gly ₃₄	2.89 ± 0.24	110.3 ± 7.75	−52.07	−27.88
Chi ₁₃ FG ₅₃ Gly ₃₄	6.03 ± 0.46	152.95 ± 8.85	reference	reference

**Figure 6.** Indicative stress vs strain plots of the hydrogel membranes Chi₂₀FG₂₀ChS₅Gly₅₅ (a), Chi₁₇FG₃₄ChS₄Gly₄₅ (b), Chi₁₃FG₅₀ChS₃Gly₃₄ (c) and Chi₁₃FG₅₃Gly₃₄ (d).

2.6. SEM Measurements

SEM was used to study the influence of the synthetic procedure and the incorporation of ChS on the surface morphology of the hydrogel membranes. Representative surface and cross section SEM images of the hydrogel membranes Chi₂₀FG₂₀ChS₅Gly₅₅ (a), Chi₁₇FG₃₄ChS₄Gly₄₅ (b), Chi₁₃FG₅₀ChS₃Gly₃₄ (c) and Chi₁₃FG₅₃Gly₃₄ (d) are illustrated in Figure 7. All the samples show dense morphology, while no pores or voids are observed. The solvent evaporation method used to develop the hydrogel membranes is an effective method for the development of hydrogel membranes with continuous and dense structure.

2.7. Water Uptake

Water uptake constitutes an important characteristic in wound dressings because a moist environment is required to enhance wound healing and to avoid dehydration in the wound area [32]. In the present study, the water uptake results are expressed as Swelling Ratio (%) and are shown in Figure 8. The results verify the important role of chondroitin sulfate in water uptake ability. The swelling ratio of the hydrogel membranes Chi₂₀FG₂₀ChS₅Gly₅₅ (Figure 8a), Chi₁₇FG₃₄ChS₄Gly₄₅ (Figure 8b), Chi₁₃FG₅₀ChS₃Gly₃₄ (Figure 8c) and Chi₁₃FG₅₃Gly₃₄ (Figure 8d) is 209%, 294%, 462% and 186%, respectively.

Comparing the results depicted in Figure 8c with the results in Figure 8d, it is clear that the incorporation of chondroitin sulfate led to increased water uptake ability due to the hydrophilic nature of the natural polymer ChS. As can be seen from Table 2, the sample Chi₁₃FG₅₀ChS₃Gly₃₄ contains the highest concentration of fish gelatin. The higher water uptake capacity of that sample is attributed to the hydrophilicity of fish gelatin [16].

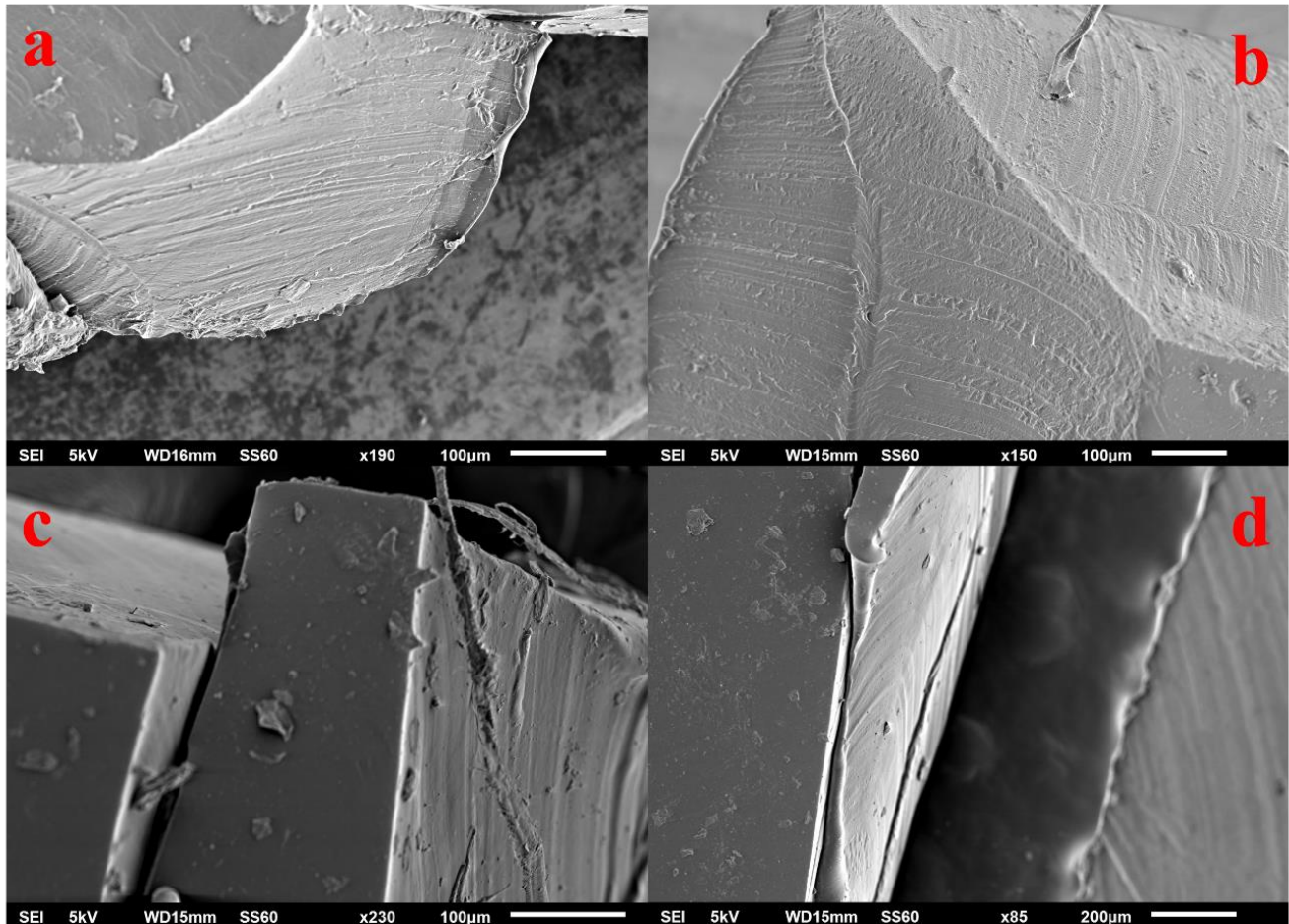


Figure 7. Cross sectional SEM images of Chi₂₀FG₂₀ChS₅Gly₅₅ (a), Chi₁₇FG₃₄ChS₄Gly₄₅ (b), Chi₁₃FG₅₀ChS₃Gly₃₄ (c) and Chi₁₃FG₅₃Gly₃₄ (d) hydrogel membrane.

Table 2. Code names and compositions of the hydrogel membranes.

Sample Code	Chitosan (w/v)	Fish Gelatin (w/v)	Chondroitin Sulfate (w/v)	Glycerol (v/v)
Chi ₂₀ FG ₂₀ ChS ₅ Gly ₅₅ (% wt. 20/20/5/55)	2%	2%	0.03%	4%
Chi ₁₇ FG ₃₄ ChS ₄ Gly ₄₅ (% wt. 17/34/4/45)	2%	4%	0.03%	4%
Chi ₁₃ FG ₅₀ ChS ₃ Gly ₃₄ (% wt. 13/50/3/34)	2%	8%	0.03%	4%
Chi ₃₀ Gly ₇₀ (% wt. 30/70)	2%	-	-	4%
Chi ₁₃ FG ₅₃ Gly ₃₄ (% wt. 13/53/34)	2%	8%	-	4%

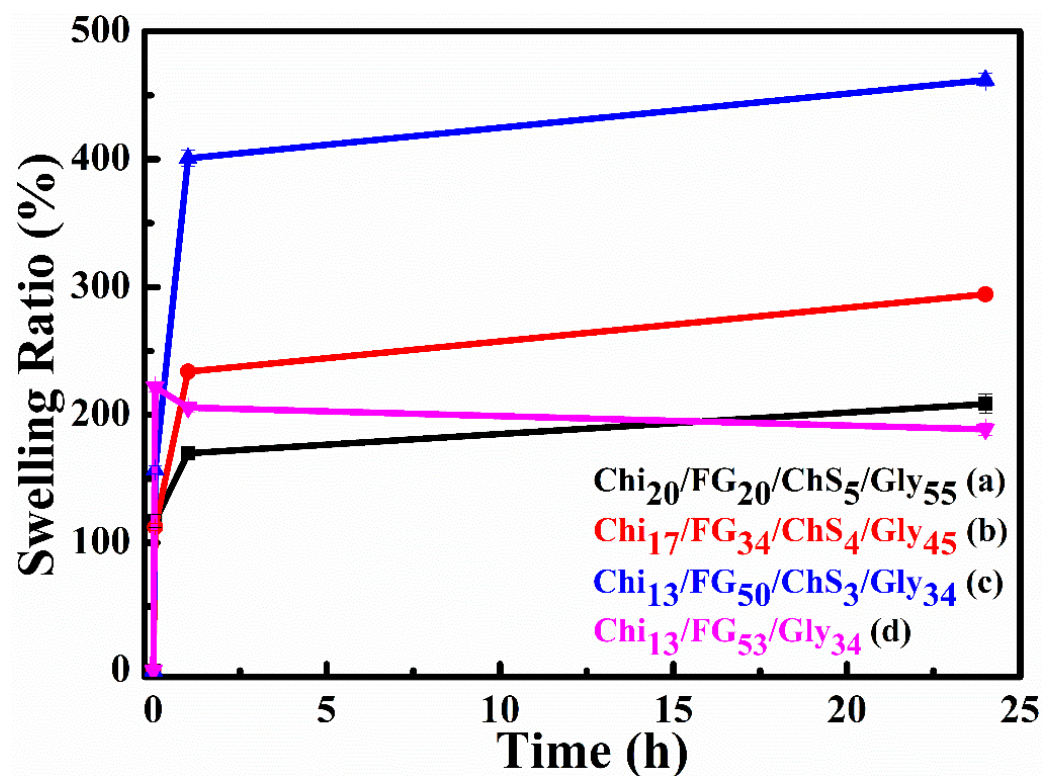


Figure 8. Swelling rate of Chi₂₀FG₂₀ChS₅Gly₅₅ (a), Chi₁₇FG₃₄ChS₄Gly₄₅ (b), Chi₁₃FG₅₀ChS₃Gly₃₄ (c) and Chi₁₃FG₅₃Gly₃₄ (d) hydrogel membrane.

2.8. Degradation Rate

Degradation rate (%) results of the current study are presented in Figure 9. It is obvious from this figure that the higher the fish gelatin concentration the higher the degradation rates. This phenomenon occurs because of fish gelatin high solubility in water. The fish-gelatin concentration increase cause an increase of non-active functional groups in the blend. Thus, no hydrogen bonds formed with chitosan, chondroitin sulfate and glycerol groups. The degradation rates were further increased after the addition of ChS. The higher degradation rate (93% mass loss the 10th day) exhibited by the Chi₁₃FG₅₀ChS₃Gly₃₄ membrane while the ChS free membrane Chi₁₃FG₅₃Gly₃₄ showed reduced degradation rate (67% mass loss the 10th day). The higher degradation rate observed for the Chi₁₃FG₅₀ChS₃Gly₃₄ relative to Chi₁₃FG₅₃Gly₃₄ membrane is maybe attributed to poor miscibility of the blend components after the integration of ChS due to lack of binding sites.

2.9. Water Vapor Transmission Rate (WVTR)

The results of Water Vapor Transmission Rate (WVTR) measurements interpretation are presented in Figure 10. For the Chi₂₀FG₂₀ChS₅Gly₅₅, Chi₁₇FG₃₄ChS₄Gly₄₅, Chi₁₃FG₅₀ChS₃Gly₃₄, and Chi₁₃FG₅₃Gly₃₄ hydrogel membranes the WVTR values are 1605, 1218, 1064, and 934 g·m⁻²·d⁻¹, respectively. The higher the fish gelatin concentration in the blends the lower the water vapor permeability. The incorporation of chondroitin sulfate with the fish gelatin increases the WVTR values comparing with the relevant WVTR values of the ChS free material (Figure 10c versus Figure 10d). The vapors permeate the ChiFGChSGly membranes through an adsorption and diffusion process [31]. According to the literature reports the WVTR values of human skin varies from 204 g·m⁻²·day⁻¹ to 5138 ± 202 g·m⁻²·day⁻¹ depending on the type and healing stage of the wound [1,31]. The WVTR values of the examined Chi_xFG_xChS_xSGly_x membranes were in the range of 1064 to 1605 g·m⁻²·day⁻¹. Such values indicate the appropriation of the examined hydrogel membranes for wound dressing.

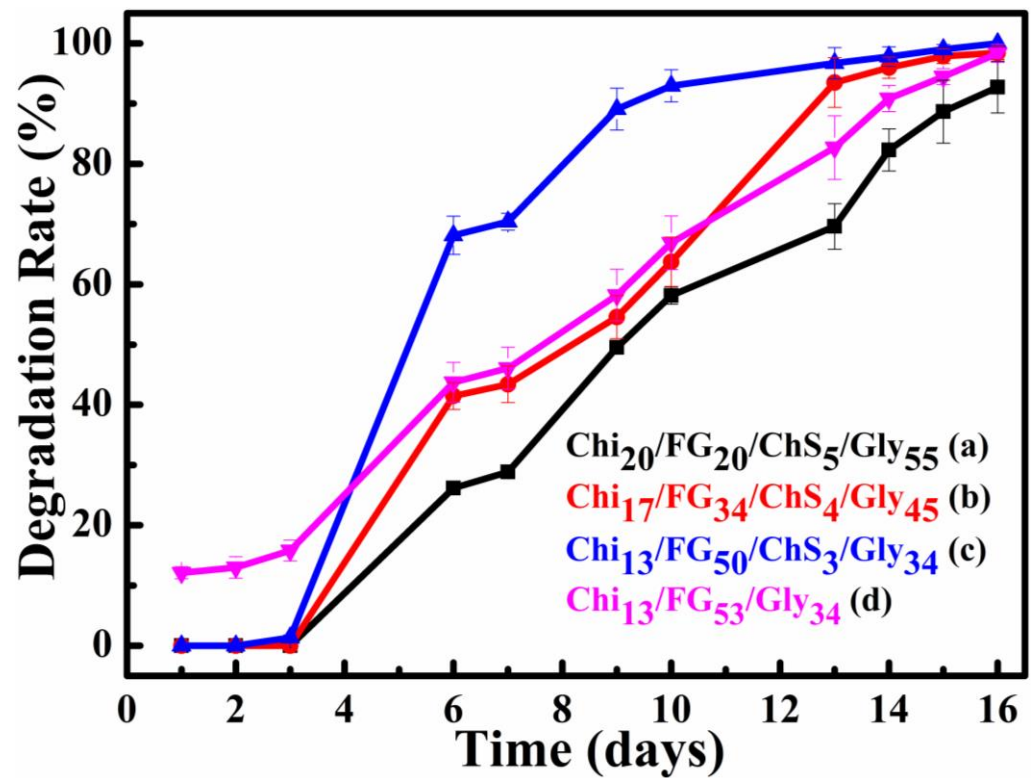


Figure 9. Degradation rate of Chi₂₀FG₂₀ChS₅Gly₅₅ (a), Chi₁₇FG₃₄ChS₄Gly₄₅ (b), Chi₁₃FG₅₀ChS₃Gly₃₄ (c) and Chi₁₃FG₅₃Gly₃₄ (d) hydrogel membrane.

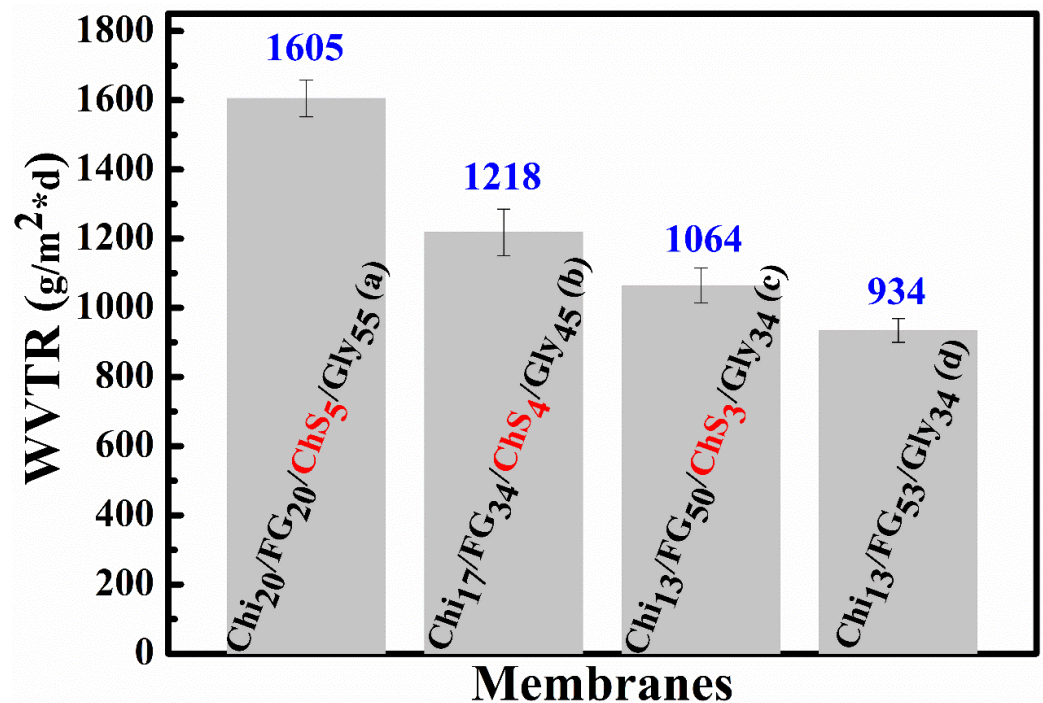


Figure 10. Water vapor transmission rate of Chi₂₀FG₂₀ChS₅Gly₅₅ (a), Chi₁₇FG₃₄ChS₄Gly₄₅ (b), Chi₁₃FG₅₀ChS₃Gly₃₄ (c) and Chi₁₃FG₅₃Gly₃₄ (d) hydrogel membranes.

2.10. Attachment of Endothelial Cells on Hydrogel Membranes In Vitro

To test the biocompatibility of the Chi₁₃FG₅₃Gly₃₄ and Chi₁₃FG₅₀ChS₃Gly₃₄ hydrogel membranes, we addressed the attachment of primary endothelial cells. The choice of

primary endothelial cells was dictated by the fact that (1) these cells are very sensitive and do not easily attach to all surfaces and (2) due to their application in regenerative medicine and tissue repair. Indeed, angiogenesis (the formation of blood vessels from pre-existing ones) is critical for tissue regeneration and normal tissue function, as blood vessels transport nutrients, oxygen and blood cells to all tissues, while removing waste materials and carbon dioxide. The endothelial cells form a single cell layer that lines all blood vessels and regulates exchanges between the bloodstream and the surrounding tissues, all cells are located within 100 to 200 μm of blood vessels—the diffusion limit for oxygen [33]. We found that endothelial cells attached successfully on both hydrogel membranes 4h after their addition, providing strong evidence that there is no cytotoxicity and allowing the further use of the membranes in in vitro and in vivo experiments. EC attachment to the $\text{Chi}_{13}\text{FG}_{50}\text{ChS}_3\text{Gly}_{34}$ membrane was statistically significantly higher ($p < 0.05$) compared to the $\text{Chi}_{15}\text{FG}_{50}\text{Gly}_{35}$ membrane as shown in Figure 11. This finding is supported by the work of Thalla et al. reporting the incorporation of chondroitin sulfate improves membrane properties by increasing endothelial cell adhesion [34–36].

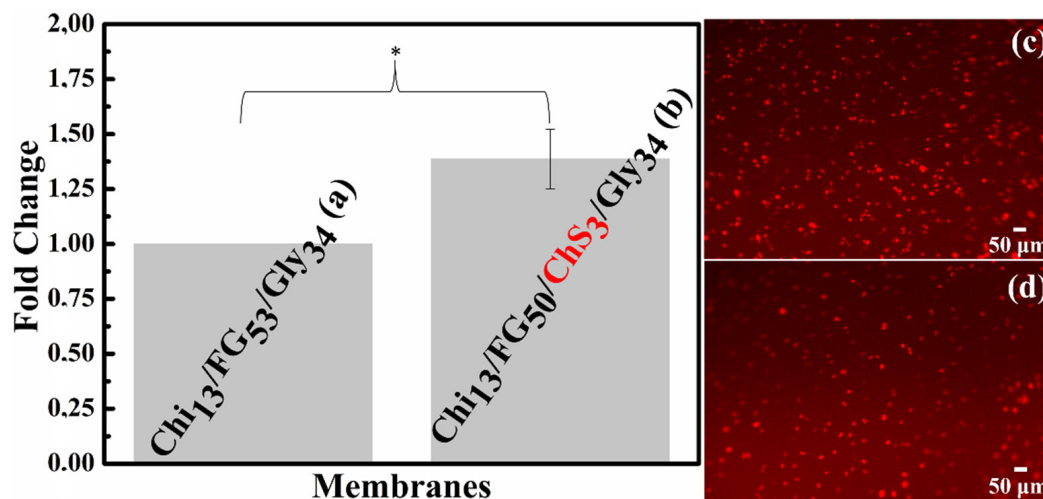


Figure 11. Attachment of Endothelial cells on $\text{Chi}_{13}\text{FG}_{53}\text{Gly}_{34}$ (a) and $\text{Chi}_{13}\text{FG}_{50}\text{ChS}_3\text{Gly}_{34}$ (b) hydrogel membranes. Numbers of attached ECs at 4 h are expressed as fold change relative to $\text{Chi}_{13}\text{FG}_{53}\text{Gly}_{34}$ membrane and presented as mean \pm SD from three independent experiments. * $p < 0.05$. Images of ECs infected with H2B-mCherry lentivirus after 4h on hydrogel membranes $\text{Chi}_{13}\text{FG}_{50}\text{ChS}_3\text{Gly}_{34}$ (c) and $\text{Chi}_{13}\text{FG}_{53}\text{Gly}_{34}$ (d).

3. Conclusions

In the present study, hydrogel membranes of dense chitosan/fish gelatin/chondroitin sulfate/glycerol were synthesized. The solution casting-evaporation procedure was adopted for this synthesis and the use of chemical crosslinkers was rejected because of their potential cytotoxicity effects. Materials' properties changed because of the chondroitin sulfate addition and the effect of its integration in the final product was evaluated. The increase of fish gelatin content as well as the incorporation of chondroitin sulfate in the blend, led to increased water uptake ability. Furthermore, the integration of chondroitin sulfate, led to increase in WVTR and degradation rate. The attachment of endothelial cells was supported by both the hydrogel membranes $\text{Chi}_{13}\text{FG}_{53}\text{Gly}_{34}$ and $\text{Chi}_{13}\text{FG}_{50}\text{ChS}_3\text{Gly}_{34}$, confirming that there is no cytotoxicity, and the ChS containing membrane showed enhanced endothelial cell attachment. Finally, as indicated from the overall materials' properties, the effective wound dressing and wound healing could be achieved using the product proposed in this study.

4. Materials and Methods

4.1. Materials

Sigma–Aldrich (St. Louis, MO, USA) was the supplier of medium molecular weight chitosan (75–85% deacetylated), cold water fish skin derived gelatin, glycerol, heparin, and dPBS (dulbecco’s Phosphate Buffered Saline). Acros Organics chondroitin sulfate sodium salt (Geel, Belgium) was also purchased for this project needs. Honeywell Fluka Research Chemicals (Charlotte, NC, USA) was the supplier for acetic acid while M199, fetal bovine serum (FBS) and penicillin–streptomycin were purchased from Gibco™—Thermo Fisher Scientific (Waltham, MA, USA). Calcein provided by eBioscience (San Diego, CA, USA) and lentivirus production H2B-mCherry plasmid provided from Addgene (Watertown, MA, USA) were also used for project’s purposes.

4.2. Hydrogel Membrane Synthesis

For the $\text{Chi}_{20}\text{FG}_{20}\text{ChS}_5\text{Gly}_{55}$ hydrogel membrane synthesis, in a beaker A (Figure 12) containing 19 mL of distilled water, 0.5 g of fish gelatin was added and allowed to stir until completely dissolved. Then, while stirring the solution, 0.5 g of chitosan was added followed by the addition of 4% (*v/v*) acetic acid. The solution was left to stir for 10 min. In a second beaker B (Figure 12), 0.125 g of chondroitin sulfate were dissolved in 5 mL of water and this solution was then added dropwise to beaker A (Figure 12), under stirring. After the addition of chondroitin sulfate the solution turned from pale yellow and clear to white translucent. The transformation of the solution from clear to translucent is attributed to the formation of polyelectrolyte [20]. Subsequently 4% (*v/v*) glycerol was added, and the solution remained under stirring overnight. The final solution contains 0.5 g (2% *w/v*) fish gelatin, 0.5 g (2% *w/v*) chitosan, 0.125 g (0.031% *w/v*) chondroitin sulfate and 1.26 g (4% *v/v*) glycerol. The solution is then placed in an ultrasonic bath for 30 min in degas mode to remove the bubbles. It is then transferred to polystyrene plates to evaporate the solvent and form the hydrogel membrane. The same procedure was followed for the synthesis of the rest of materials and the synthetic procedure of $\text{Chi}_{13}\text{FG}_{53}\text{Gly}_{34}$ is the same but without the addition of ChS. The quantities used are listed in Table 2 and the synthesis is illustrated in Figure 12.

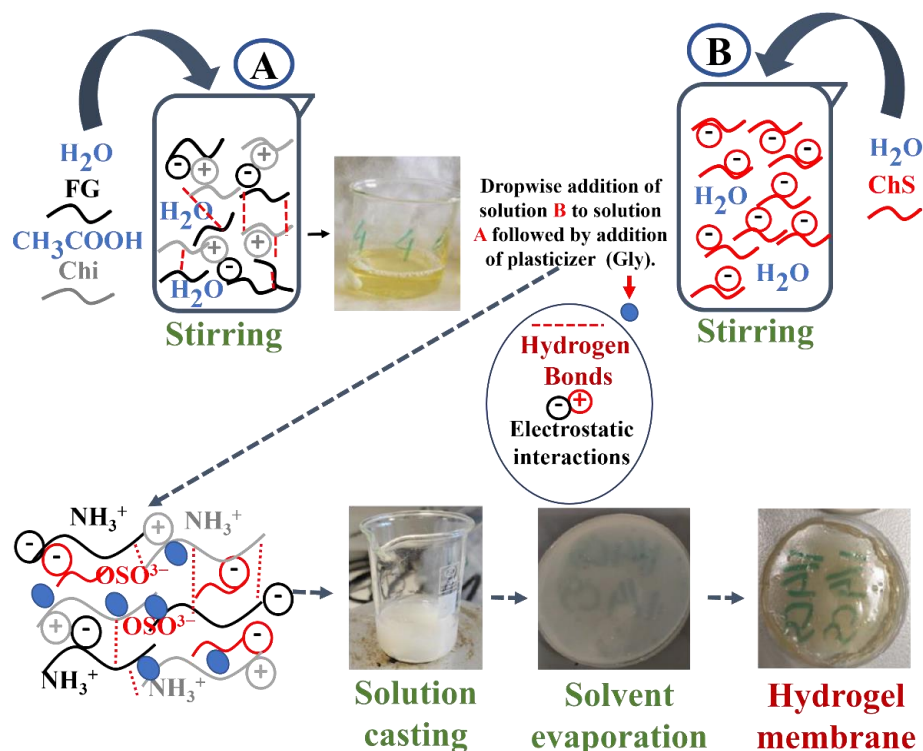


Figure 12. Schematic illustration of hydrogel membranes synthesis.

4.3. ATR-FTIR Analysis

A coupled instrument, of Jasco FT/IR-4100 spectrometer (JASCO, Interlab, S.A., Athens, Greece) and Jasco IRT-5000 microscope (JASCO, Interlab, S.A., Athens, Greece), was used to carry out ATR-FTIR measurements on the prepared membranes characterization. ATR device of the instrument includes a ZnSe prism with a 250 μm contact area, around 2.0 μm (@1000 cm^{-1}) penetration depth, and capable for measurements down to 650 cm^{-1} .

4.4. XRD Analysis

A PANalytical X'PertPRO diffractometer was employed for XRD crystallinity measurements using $\text{CoK}\alpha$ radiation. The X'Celerator detector of this instrument was operated at 40 kV voltage and 40 mA current. The 2θ range 2° – 60° was scanned on all membrane samples.

4.5. Thermogravimetric Analysis (TGA)

Setsys Evolution- Setaram thermogravimetric instrument was used for TGA, TG-DSC, and TG-DTA analysis of ~30 mg of sample placed in a platinum crucible. All tested samples were heated from ambient to 700 $^\circ\text{C}$ with a temperature increasing rate of 10 $^\circ\text{C}\cdot\text{min}^{-1}$ while the gas (N_2) flow rate was set at 25 $\text{mL}\cdot\text{min}^{-1}$.

4.6. Dynamic Mechanical Analysis (DMA)

Thermomechanical properties were determined using a Q800 (TA Instruments, New Castle, DE, USA) instrument in film tension mode and a deformation amplitude set at 15 μm . Storage modulus (E') and loss factor ($\tan\delta$) were estimated scanning the temperature range from -70°C to 120 $^\circ\text{C}$ with a temperature increasing rate of 3 $^\circ\text{C}/\text{min}$ and a frequency of 1 Hz.

4.7. Mechanical Properties

ASTM D638 standard was adopted to evaluate the tensile properties of the different membranes. A hand made horizontal tensile testing stage was used. Samples were cut to type V dumbbell shape and a 0.1 min^{-1} strain rate was applied to tested samples until failure. A linear variable differential transformer (LVDT) was used to record the elongation of each specimen. Three independent samples per each type of membrane were tested using a 44.5 N load cell (or a 445 N load cell for the pure specimens) to measure the load. According to theory and Equation (1), strain was calculated by dividing the elongation values with the initial effective length of each specimen.

$$\text{strain} = \frac{\Delta\ell}{\ell_0} \quad (1)$$

where $\Delta\ell$ is the elongation value and ℓ the initial effective length.

Similarly, according to theory and Equation (2), stress was estimated by dividing the load values with the cross-sectional area of each specimen.

$$\sigma = \frac{F}{S} \quad (2)$$

where F is the load applied to the sample for elongation and S is the cross-sectional area of the sample.

4.8. Scanning Electron Microscopy (SEM)

JEOL JSM-6510 LV (JEOL Ltd., Tokyo, Japan) SEM instrument was employed to characterize the surface structure of the samples by the applications of 5 kV acceleration voltage. For such characterizations an equipped X-Act EDS-detector (Abingdon, Oxford Instruments, Oxfordshire, UK) was used. To avoid samples charging the membranes were firstly sputter-coated with gold in vacuum for 30 s, and a 5 kV acceleration voltage was applied for the examination tests.

4.9. Water Uptake Study

Circular disk shape samples of 12 mm diameter were tested for the water uptake ability. Membranes were immersed in distilled water and the swelling property was estimated by immediately weighing at 3 min, 1 h, and 24 h after the excess water removal using a filter paper as absorbant material. Equation (3) was used for the membranes' swelling ability estimation.

$$SR = \frac{W_s - W_d}{W_d} \quad (3)$$

where SR is the swelling ratio, W_s is the weight of the membrane measured at each specific time point, and W_d is the initial weight of the membrane. Swelling ratio (SR) is the indicative value of the swelling ability.

4.10. Degradation Rate Study

Degradation rate study of hydrogel membranes was carried out by systematic measuring of the weight loss of samples. Circular disk shape samples of 12 mm diameter and initial weight m_0 were immersed in 5 mL of distilled water and weighted after the 1st, 2nd, 3rd, 6th, 7th, 9th, 10th, 13th, 14th, 15th and 16th day. Weighing carried out after the excess water removal with filter paper as absorbant. The (%) degradation rate was determined according to Equation (4).

$$\% \text{ degradation} = \frac{m_0 - m_i}{m_0} \times 100 \quad (4)$$

where m_0 is initial mass of the hydrogel membrane and m_i is the mass of the membrane at the end of the i th day.

4.11. Water Vapor Permeability

Membranes were placed on top of the circular mouth of glass bottles contained 5 mL of distilled water. The mouth perimeter was sealed using commercial glue and the water-vapor permeability of membranes was estimated according to a procedure reported in literature [31]. The water vapor transmission rate measurements were carried out at 37 °C and calculated according to the Equation (5).

$$WVTR = \frac{W_i - W_0}{t \cdot A} \quad (5)$$

where WVTR is the Water Vapor Transmission Rate ($\text{g} \cdot \text{m}^{-2} \cdot \text{d}^{-1}$), W_i is the weight of the handmade device at specific time t_i , W_0 is the initial mass of the system ($t_0 = 0$), and A is the cross-sectional area of the glass bottle mouth.

4.12. Attachment of Endothelial Cells, In Vitro, on Hydrogel Membranes ECs Adhesion Assay

Human endothelial cells (ECs) originated from an umbilical vein (HUVECs) source via an isolation method which was described previously [33]. Such cells were cultivated in M199 basal medium using 20% fetal bovine serum and 30 $\mu\text{g}/\text{mL}$ endothelial cell growth (ECGS) as supplement, 4.7 U/mL heparin and 1% penicillin-streptomycin. Cells were passaged at a ratio of 1 to 3 and were used up to passage 3. After the isolation cells were infected with a H2B-mCherry lentivirus, which imparts a red fluorescent nuclear signal. Lentiviral particles were prepared according to standard protocols. The $\text{Chi}_{13}\text{FG}_{50}\text{ChS}_3\text{Gly}_{34}$ and $\text{Chi}_{13}\text{FG}_{53}\text{Gly}_{34}$ hydrogel membranes were cut into 6mm diameter pieces, washed twice for 30 min with dPBS (dulbecco's Phosphate Buffered Saline and placed into a 24-well culture plate. 30,000 HUVECs infected with H2B-mCherry lentivirus were added to each well and cultured at 37 °C, 5% CO_2 . 4 h later the medium was changed to remove unattached cells and images of attached ECs were taken using a Leica DM IRBE fluorescence microscope. The number of attached cells was measured using ImageJ software. Three independent experiments were performed. The relative number of attached cells on the

two polymeric hydrogel membranes from three independent experiments were expressed as mean \pm the standard deviation value.

Statistical analysis was performed using SPSS 22.0 (SPSS, Inc). Normality tests were applied to all measurement variables. The one-way analysis of variance (ANOVA) was used for comparison between the two membranes and obtained significant probability values were also corrected for multiple testing (Bonferroni correction). Cell attachment at 4 h for each membrane was analysed using paired *t*-test. *p*, 0.05 was accepted as the level of statistical significance.

Author Contributions: Synthesis experiment design, A.K.-M., N.E.Z. and C.E.S.; characterization measurements and interpretation, A.K.-M., N.E.Z., D.M., A.A., C.G., K.T., A.E.G., E.B. and C.M.; paper writing, A.K.-M., N.E.Z. and C.E.S.; overall evaluation of this work, N.E.Z. and A.K.-M.; experimental data analysis and interpretation N.E.Z., C.E.S., A.K.-M.; TGA, M.A.K. and C.G., Tensile measurements, K.T. and A.P., SEM measurements, D.M. and A.A. In vitro endothelial cells colonization tests, M.M., E.B. and C.M. All authors have read and agreed to the published version of the manuscript.

Funding: This research was co-financed by Greece and the European Union (European Social Fund—ESF) through the Operational Programme “Human Resources Development, Education and Lifelong Learning” in the context of the project “Strengthening Human Resources Research Potential via Doctorate Research” (MIS-5000432), implemented by the State Scholarships Foundation (IJT).

Institutional Review Board Statement: Not applicable.

Informed Consent Statement: Not applicable.

Data Availability Statement: The datasets generated for this study are available on request to the corresponding author.

Conflicts of Interest: The authors declare no conflict of interest.

References

1. Negut, I.; Dorcioman, G.; Grumezescu, V. Scaffolds for Wound Healing Applications. *Polymers* **2020**, *12*, 2010. [[CrossRef](#)] [[PubMed](#)]
2. Jannesari, M.; Varshosaz, J.; Morshed, M.; Zamani, M. Composite poly(vinyl alcohol)/poly(vinyl acetate) electrospun nanofibrous mats as a novel wound dressing matrix for controlled release of drugs. *Int. J. Nanomed.* **2011**, *6*, 993–1003. [[CrossRef](#)]
3. Talikowska, M.; Fu, X.; Lisak, G. Application of conducting polymers to wound care and skin tissue engineering: A review. *Biosens. Bioelectron.* **2019**, *135*, 50–63. [[CrossRef](#)] [[PubMed](#)]
4. Day, R.M. *Advanced Wound Repair Therapies*, 1st ed.; Farrar, D., Ed.; Woodhead Publishing: Cambridge, UK, 2011; pp. 155–173.
5. Field, C.K.; Kerstein, M.D. Overview of wound healing in a moist environment. *Am. J. Surg.* **1994**, *167*, S2–S6. [[CrossRef](#)] [[PubMed](#)]
6. Kamoun, E.A.; Kenawy, E.-R.S.; Chen, X. A review on polymeric hydrogel membranes for wound dressing applications: PVA-based hydrogel dressings. *J. Adv. Res.* **2017**, *8*, 217–233. [[CrossRef](#)] [[PubMed](#)]
7. Liu, H.; Wang, C.; Li, C.; Qin, Y.; Wang, Z.; Yang, F.; Li, Z.; Wang, J. A functional chitosan-based hydrogel as a wound dressing and drug delivery system in the treatment of wound healing. *RSC Adv.* **2018**, *8*, 7533–7549. [[CrossRef](#)] [[PubMed](#)]
8. Hu, H.; Xu, F.-J. Rational design and latest advances of polysaccharide-based hydrogels for wound healing. *Biomater. Sci.* **2020**, *8*, 2084–2101. [[CrossRef](#)]
9. Oryan, A.; Kamali, A.; Moshiri, A.; Baharvand, H.; Daemi, H. Chemical crosslinking of biopolymeric scaffolds: Current knowledge and future directions of crosslinked engineered bone scaffolds. *Int. J. Biol. Macromol.* **2018**, *107*, 678–688. [[CrossRef](#)]
10. Tabor, R.F.; Grieser, F.; Dagastine, R.R.; Chan, D.Y.C. The hydrophobic force: Measurements and methods. *Phys. Chem. Chem. Phys.* **2014**, *16*, 18065–18075. [[CrossRef](#)]
11. Mogoşanu, G.D.; Grumezescu, A.M. Natural and synthetic polymers for wounds and burns dressing. *Int. J. Pharm.* **2014**, *463*, 127–136. [[CrossRef](#)]
12. Zhong, S.P.; Zhang, Y.Z.; Lim, C.T. Tissue scaffolds for skin wound healing and dermal reconstruction. *Wiley Interdiscip. Rev. Nanomed. Nanobiotechnology* **2010**, *2*, 510–525. [[CrossRef](#)] [[PubMed](#)]
13. Fajardo, A.R.; Laís, C.; Lopes, L.C.; Caleare, A.O.; Britta, E.A.; Nakamura, C.V.; Rubira, A.F.; Muniz, E.C. Silver sulfadiazine loaded chitosan/chondroitin sulfate films for a potential wound dressing application. *Mater. Sci. Eng. C* **2013**, *33*, 588–595. [[CrossRef](#)] [[PubMed](#)]
14. Liu, Y.; Dong, T.; Chen, Y.; Sun, N.; Liu, Q.; Huang, Z.; Yang, Y.; Cheng, H.; Yue, K. Biodegradable and Cytocompatible Hydrogel Coating with Antibacterial Activity for the Prevention of Implant-Associated Infection. *ACS Appl. Mater. Interfaces* **2023**, *15*, 11507–11519. [[CrossRef](#)] [[PubMed](#)]

15. Lu, J.; Chen, Y.; Ding, M.; Fan, X.; Hu, J.; Chen, Y.; Li, J.; Li, Z.; Liu, W. A 4arm-PEG macromolecule crosslinked chitosan hydrogels as antibacterial wound dressing. *Carbohydr. Polym.* **2022**, *277*, 118871. [[CrossRef](#)] [[PubMed](#)]
16. Karydis-Messinis, A.; Moschovas, D.; Markou, M.; Gkantou, E.; Vasileiadis, A.; Tsirka, K.; Gioti, C.; Vasilopoulos, K.C.; Bagli, E.; Murphy, C.; et al. Development, physicochemical characterization and in vitro evaluation of chitosan-fish gelatin-glycerol hydrogel membranes for wound treatment applications. *Carbohydr. Polym. Technol. Appl.* **2023**, *6*, 100338. [[CrossRef](#)]
17. Charbonneau, C.; Liberelle, B.; Hébert, M.-J.; De Crescenzo, G.; Lerouge, S. Stimulation of cell growth and resistance to apoptosis in vascular smooth muscle cells on a chondroitin sulfate/epidermal growth factor coating. *Biomaterials* **2011**, *32*, 1591–1600. [[CrossRef](#)] [[PubMed](#)]
18. Zhou, F.; Zhang, X.; Cai, D.; Li, J.; Mu, Q.; Zhang, W.; Zhu, S.; Jiang, Y.; Shen, W.; Zhang, S.; et al. Silk fibroin-chondroitin sulfate scaffold with immuno-inhibition property for articular cartilage repair. *Acta Biomater.* **2017**, *63*, 64–75. [[CrossRef](#)] [[PubMed](#)]
19. Lamme, E.N.; de Vries, H.J.; van Veen, H.; Gabbiani, G.; Westerhof, W.; Middelkoop, E. Extracellular matrix characterization during healing of full-thickness wounds treated with a collagen/elastin dermal substitute shows improved skin regeneration in pigs. *J. Histochem. Cytochem. Off. J. Histochem. Soc.* **1996**, *44*, 1311–1322. [[CrossRef](#)]
20. Sharma, S.; Swetha, K.L.; Roy, A. Chitosan-Chondroitin sulfate based polyelectrolyte complex for effective management of chronic wounds. *Int. J. Biol. Macromol.* **2019**, *132*, 97–108. [[CrossRef](#)]
21. Fialkova, M.A.; Smirnova, T.; Ivanova, G.I.; Aboians, R.K.; Golubeva, V.F. The effect of chondroitin sulfate preparations on wound healing and the strength of the surgical scar. *Biulleten' Eksperimental'noi Biol. I Meditsiny* **1989**, *108*, 350–351. [[CrossRef](#)]
22. Pan, Y.; Xiao, C.; Tan, H.; Yuan, G.; Li, J.; Li, S.; Jia, Y.; Xiong, D.; Hu, X.; Niu, X. Covalently injectable chitosan/chondroitin sulfate hydrogel integrated gelatin/heparin microspheres for soft tissue engineering. *Int. J. Polym. Mater. Polym. Biomater.* **2021**, *70*, 149–157. [[CrossRef](#)]
23. S, P.; Jaiswal, A.K. Effect of interpolymer complex formation between chondroitin sulfate and chitosan-gelatin hydrogel on physico-chemical and rheological properties. *Carbohydr. Polym.* **2020**, *238*, 116179. [[CrossRef](#)]
24. Ng, W.L.; Yeong, W.Y.; Naing, M.W. Development of Polyelectrolyte Chitosan-gelatin Hydrogels for Skin Bioprinting. *Procedia CIRP* **2016**, *49*, 105–112. [[CrossRef](#)]
25. Ng, W.L.; Yeong, W.Y.; Win Naing, M. Polyelectrolyte gelatin-chitosan hydrogel optimized for 3D bioprinting in skin tissue engineering. *Int. J. Bioprint.* **2016**, *2*, 53–62. [[CrossRef](#)]
26. Criado, M.; Rey, J.M.; Mijangos, C.; Hernández, R. Double-membrane thermoresponsive hydrogels from gelatin and chondroitin sulphate with enhanced mechanical properties. *RSC Adv.* **2016**, *6*, 105821–105826. [[CrossRef](#)]
27. Venkatesan, J.; Pallela, R.; Bhatnagar, I.; Kim, S.-K. Chitosan-amylopectin/hydroxyapatite and chitosan-chondroitin sulphate/hydroxyapatite composite scaffolds for bone tissue engineering. *Int. J. Biol. Macromol.* **2012**, *51*, 1033–1042. [[CrossRef](#)] [[PubMed](#)]
28. Wang, S.-J.; Wang, B.-B.; Bai, F.-W.; Ma, X.-J. Tumor cell responses to carbon dots derived from chondroitin sulfate. *RSC Adv.* **2015**, *5*, 81388–81394. [[CrossRef](#)]
29. Arvanitoyannis, I.S.; Nakayama, A.; Aiba, S.-i. Chitosan and gelatin based edible films: State diagrams, mechanical and permeation properties. *Carbohydr. Polym.* **1998**, *37*, 371–382. [[CrossRef](#)]
30. Matveev, Y.I.; Grinberg, V.Y.; Tolstoguzov, V.B. The plasticizing effect of water on proteins, polysaccharides and their mixtures. Glassy state of biopolymers, food and seeds. *Food Hydrocoll.* **2000**, *14*, 425–437. [[CrossRef](#)]
31. Ma, Y.; Xin, L.; Tan, H.; Fan, M.; Li, J.; Jia, Y.; Ling, Z.; Chen, Y.; Hu, X. Chitosan membrane dressings toughened by glycerol to load antibacterial drugs for wound healing. *Mater. Sci. Eng. C* **2017**, *81*, 522–531. [[CrossRef](#)]
32. Junker, J.P.; Kamel, R.A.; Caterson, E.J.; Eriksson, E. Clinical Impact Upon Wound Healing and Inflammation in Moist, Wet, and Dry Environments. *Adv. Wound Care* **2013**, *2*, 348–356. [[CrossRef](#)]
33. Kostopoulou, N.; Bellou, S.; Bagli, E.; Markou, M.; Kostaras, E.; Hyvönen, M.; Kalaidzidis, Y.; Papadopoulos, A.; Chalmantzi, V.; Kyrkou, A.; et al. Embryonic stem cells are devoid of macropinocytosis, a trafficking pathway for activin A in differentiated cells. *J. Cell Sci.* **2021**, *134*, jcs246892. [[CrossRef](#)]
34. Kong, X.; He, Y.; Zhou, H.; Gao, P.; Xu, L.; Han, Z.; Yang, L.; Wang, M. Chondroitin Sulfate/Polycaprolactone/Gelatin Electrospun Nanofibers with Antithrombogenicity and Enhanced Endothelial Cell Affinity as a Potential Scaffold for Blood Vessel Tissue Engineering. *Nanoscale Res. Lett.* **2021**, *16*, 62. [[CrossRef](#)]
35. Ma, L.; Li, X.; Guo, X.; Jiang, Y.; Li, X.; Guo, H.; Zhang, B.; Xu, Y.; Wang, X.; Li, Q. Promotion of Endothelial Cell Adhesion and Antithrombogenicity of Polytetrafluoroethylene by Chemical Grafting of Chondroitin Sulfate. *ACS Appl. Bio Mater.* **2020**, *3*, 891–901. [[CrossRef](#)]
36. Thalla, P.K.; Fadlallah, H.; Liberelle, B.; Lequoy, P.; De Crescenzo, G.; Merhi, Y.; Lerouge, S. Chondroitin sulfate coatings display low platelet but high endothelial cell adhesive properties favorable for vascular implants. *Biomacromolecules* **2014**, *15*, 2512–2520. [[CrossRef](#)]

Disclaimer/Publisher's Note: The statements, opinions and data contained in all publications are solely those of the individual author(s) and contributor(s) and not of MDPI and/or the editor(s). MDPI and/or the editor(s) disclaim responsibility for any injury to people or property resulting from any ideas, methods, instructions or products referred to in the content.